



OPEN

Interaction-induced localization of mobile impurities in ultracold systems

Jian Li¹, Jin An^{1,2} & C. S. Ting¹

¹Texas Center for Superconductivity and Department of Physics, University of Houston, Houston, Texas 77204, USA, ²National Laboratory of Solid State Microstructures and Department of Physics, Nanjing University, Nanjing 210093, China.

SUBJECT AREAS:
EXOTIC ATOMS AND
MOLECULES
ULTRACOLD GASES

Received
11 January 2013

Accepted
21 October 2013

Published
6 November 2013

Correspondence and
requests for materials
should be addressed to
C.S.T. (ting@uh.edu)

The impurities, introduced intentionally or accidentally into certain materials, can significantly modify their characteristics or reveal their intrinsic physical properties, and thus play an important role in solid-state physics. Different from those static impurities in a solid, the impurities realized in cold atomic systems are naturally mobile. Here we propose an effective theory for treating some unique behaviors exhibited by ultracold mobile impurities. Our theory reveals the interaction-induced transition between the extended and localized impurity states, and also explains the essential features obtained from several previous models in a unified way. Based on our theory, we predict many intriguing phenomena in ultracold systems associated with the extended and localized impurities, including the formation of the impurity-molecules and impurity-lattices. We hope this investigation can open up a new avenue for the future studies on ultracold mobile impurities.

The experimental studies of impurities in the cold atomic systems^{1–5} has generated a lot of interests in this research area. It provides great opportunities for simulating the static impurity effects which have been shown in solid-state systems, like the pair-breaking effects and in-gap bound states^{6–8}. On the other hand, the impurity atoms with mobility possess strikingly unusual effects. This sparks many novel phenomena which are hard to realize in solid materials, such as attractive^{9,10} or repulsive^{11,12} Fermi polarons and quantum flutter¹³. All these push the study of the impurity effects into new prospects. Moreover, compared to the systems in real materials, the physical quantities are easier to control with cold atoms. Specifically, the impurity-background (IB) interaction can be precisely tunable in the experiments with the help of an external magnetic field^{4,5}, which facilitates exploring the exotic impurity physics with cold atoms.

The localized impurities, in analogy with the strong coupling polarons in solids¹⁴, were previously studied in several cold atomic systems, including a Bose-Einstein condensate with one or several bosonic impurities^{15–19}, a superfluid Fermi gas with small number of bosonic impurities²⁰ and a Larkin-Ovchinnikov superfluid with fermionic impurities²¹. The extended to localized transition (ELT) of the impurity state is shown to have many outstanding features: (1) Finite value of IB interaction is needed for the localization of the impurity atoms in two and three dimensions (2D and 3D)^{15,16,20,21}. (2) Any small IB interaction results in the localization of the impurity in one dimension (1D)^{17,19}. (3) The critical IB interaction for the localization of N ($N > 1$) bosonic impurities is smaller than that of a single impurity¹⁸. These features are shared or partly shared in different systems, implying some common behaviors exist in the IB interaction-induced localization of mobile impurities. In this paper, we propose a phenomenological model that is able to explain all the features listed above, and in addition, we predict some exotic features from this model that could be realizable in experiments with ultracold mobile impurities. Although our effective model is proposed for cold atomic systems, it can be extended straightforwardly to other systems with direct IB interactions. Thus our theory provides a general framework for understanding problems associated with the interaction-induced localization of mobile impurities.

Results

The effective model. As shown in the Methods section, the impurities of a total number N immersed in a background with a contact interaction can be effectively described by a universal energy functional regardless of the impurities' statistics:

$$E[\Psi_1(\mathbf{r}) \dots \Psi_N(\mathbf{r})] = \int d\mathbf{r} \left[\sum_{i=1}^N \Psi_i^*(\mathbf{r}) \left(-\frac{\hbar^2}{2m_I} \nabla^2 \right) \Psi_i(\mathbf{r}) - \alpha n_I^2(\mathbf{r}) + \beta n_I^3(\mathbf{r}) \right] \quad (1)$$

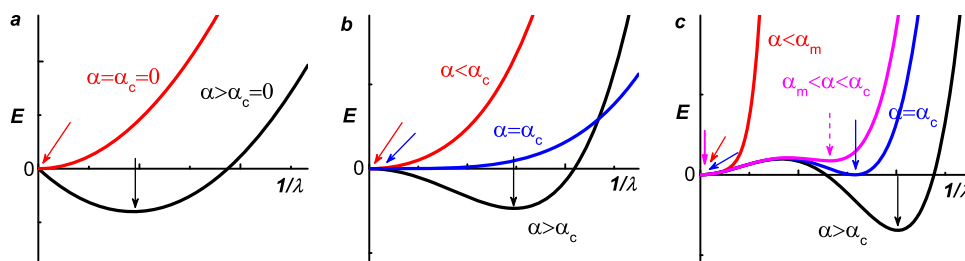


Figure 1 | Schematic diagram for single impurity energy as function of λ^{-1} with $\beta > 0$. (a–c), 1D, 2D and 3D. The arrows in solid lines indicate the global minimums of the energies, while the arrow in dashed line in (c) marks a local minimum of E .

where $n_I(\mathbf{r}) = \sum_{i=1}^N |\Psi_i(\mathbf{r})|^2$ is the local density of the impurity atoms and $\Psi_i(\mathbf{r})$ is the wave function of the i -th impurity atom. The first term in equation (1) is the kinetic energy and the last two terms are self-induced energies originating in the IB interaction. The energy minimization of equation (1) leads to the one-particle self-consistent equations for the mobile impurities:

$$\left[-\frac{\hbar^2}{2m_I} \nabla^2 - 2\alpha n_I(\mathbf{r}) + 3\beta n_I^2(\mathbf{r}) \right] \Psi_i(\mathbf{r}) = \mu_i \Psi_i(\mathbf{r}), \quad (2)$$

where μ_i are the Lagrange multipliers. The density distributions of the mobile impurities are now determined by an effective system of noninteracting atoms moving in a Kohn-Sham-like^{22,23} potential $v_{\text{eff}}(\mathbf{r}) = -2\alpha n_I(\mathbf{r}) + 3\beta n_I^2(\mathbf{r})$, and the total energy of the impurities is $E = \sum_{i=1}^N \int d\mathbf{r} \Psi_i^*(\mathbf{r}) [\mu_i + \alpha n_I(\mathbf{r}) - 2\beta n_I^2(\mathbf{r})] \Psi_i(\mathbf{r})$.

Localization of single impurity. Quantum-mechanically, for a single impurity atom confined within a length λ , its energy in l -dimension has a general form: $E \sim \frac{\hbar^2}{2m_I} \frac{1}{\lambda^2} - \frac{\alpha}{\lambda^l} + \frac{\beta}{\lambda^{2l}}$. Assuming a Gaussian trial wave function $\phi(r) = \frac{1}{(\lambda\sqrt{\pi})^{l/2}} e^{-\frac{r^2}{2\lambda^2}}$, which is similar to the Landau-Pekar treatment¹⁴ and was also used in several specific systems^{15,16}, the total energy E for a single impurity becomes

$$E = \frac{\hbar^2}{4m_I} \frac{1}{\lambda^2} - B_l \frac{\alpha}{\lambda^l} + C_l \frac{\beta}{\lambda^{2l}}, \quad (3)$$

where $B_l = (2\pi)^{-l/2}$ and $C_l = (3\pi^2)^{-l/2}$. Since thermodynamic stability requires α be positive (see Methods section), the energy contributions from the kinetic part and α -part compete with each other. In fact, the kinetic energy favors an extended state with $\lambda^{-1} = 0$ and $E = 0$, while the α -term favors a localized ground state with $\lambda = 0$ and $E = -\infty$. A positive β then stabilizes the system at a finite λ and E . The localization here is induced by the impurity itself which creates a local trap in the background through the IB interaction. Below, we show that all the essential physics about the ELT by tuning α , including the classification and the critical behaviors of the transition, are manifested in the competition of energy implied in equation (3).

As shown in Fig. 1a, a localized state with a finite λ^{-1} always gives the minimal energy E_{min} for any positive α , indicating that *the impurity is always localized in 1D*. In 2D, E_{min} appears at $\lambda^{-1} = 0$ for small α , while it appears with a negative value at a finite λ^{-1} for large α . Therefore there exists a critical value α_c above which the impurity gets localized (see Fig. 1b). At the critical point $\alpha = \alpha_c$, $\lambda_c^{-1} = 0$, indicating that *the ELT is continuous in 2D*. In 3D as illustrated in Fig. 1c, we also have $\alpha_c > 0$, but different from 2D, $\lambda_c^{-1} > 0$ at the critical point $\alpha = \alpha_c$, which suggests a *discontinuous ELT in 3D*. Additionally, there exists another critical value α_m in 3D, and in the parameter region $\alpha_m < \alpha < \alpha_c$ we have a meta-stable localized state, although the ground state is still extended.

The critical behavior of the ELT in l -dimension is then determined by $\frac{\partial E}{\partial \lambda} = 0$, and near the transition point we have the optimized localization length and energy:

$$(\lambda^{-1} - \lambda_c^{-1}) \propto (\alpha - \alpha_c)^{\nu}, \quad E \propto -(\alpha - \alpha_c)^{\delta}. \quad (4)$$

where $\nu = 1$, $\delta = 2$, $\alpha_c = 0$, $\lambda_c^{-1} = 0$ for 1D; $\nu = 1/2$, $\delta = 2$, $\alpha_c = \text{constant}$, $\lambda_c^{-1} = 0$ for 2D; $\nu = 1$, $\delta = 1$, $\alpha_c \propto \beta^{1/4}$, $\lambda_c^{-1} \propto \beta^{-1/4}$ in 3D. More precise forms of equation 4 can be found in the Supplementary Information. By solving $\frac{\partial E}{\partial \lambda} = 0$ and $\frac{\partial^2 E}{\partial \lambda^2} = 0$ simultaneously in 3D, we obtain $\alpha_m = 0.877\alpha_c$.

The exact impurity profiles and critical behaviors of the ELT can be given by solving equation (2) numerically with the centrosymmetric coordinates of the impurity state. We start with an initial guess of $n_I(\mathbf{r})$, then calculate the potential terms. By minimizing the total energy, we get the $\Psi_i(\mathbf{r})$ and a new $n_I(\mathbf{r})$. This process is repeated until the final density is converged. It also needs to make sure that the integration of $n_I(\mathbf{r})$ over the real space should yield the total number N of the impurities. To extract the universal features from the numerical results, we introduce the length/energy units and dimensionless parameters: α' and β' (see Table 1). As shown in Fig. 2a–c, there always exists a finite localization length in 1D while in 2D and 3D the localization length $\lambda \rightarrow \infty$ for small α' , implying that the impurity is always localized in 1D while a critical parameter is needed in 2D and 3D for the localization. From the energy behaviors shown in the inset-plot of Fig. 2, we can see that the ELT is continuous in 2D while discontinuous in 3D. Especially, the critical exponent δ is 1.95 for 2D and 0.99 for 3D, and the critical parameters (see Fig. 2 and its caption) from the numerical calculations are in good agreement with those from our Gaussian-trial-wave function approaches. This coincides with the conclusions drawn from several specific models, that the Gaussian trial wave function is reliable for the localized impurity state^{15,16}.

In our theory, the essential physics can be extracted by expanding the energy to the third order of the impurity density, and taking higher orders into consideration does not change the properties of the ELT as long as they contribute a positive energy. This is similar to the Ginzburg-Landau (G-L) equation where the free energy is expanded to the second order in the density of superconducting order parameter. The localization length λ , which is in analogy to the coherence length in G-L equations, characterizes the size of the localized wave packet. However, the transition here is between two different states but not phases, and the critical behavior of the transition here is strongly dimension-dependent, which are quite different from G-L theory.

Soliton excitations. The dynamics of single impurity is described by the time-dependent Schrödinger equation:

$$i\hbar \frac{\partial}{\partial t} \Psi(\mathbf{r}, t) = H_{\text{eff}} \Psi(\mathbf{r}, t) \quad (5)$$

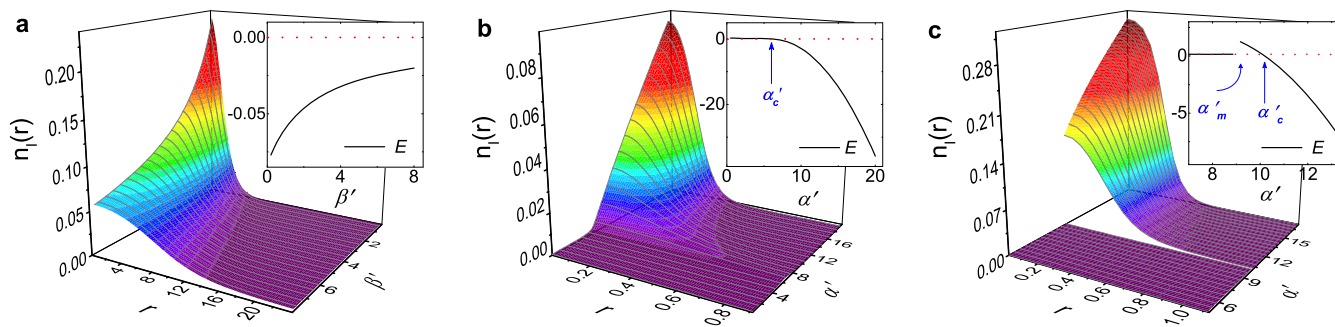


Figure 2 | The impurity structure as function of the dimensionless parameter. (a–c), 1D, 2D and 3D. The asymptotic behavior of the localized wave function indicated by equation (2) is parabolic at $r \rightarrow 0$: $\Psi(r) \rightarrow \Psi(0) + \frac{1}{2}\Psi''(0)r^2$, and exponential at $r \rightarrow \infty$: $\Psi(r) \rightarrow e^{-kr}$. Inset: The corresponding energy of the impurity as function of the dimensionless parameter in (a–c). The dashed (red) lines represent the energy of the extended states. The blue arrows mark the critical values of the dimensionless parameters for the occurrence of the localized or meta-stable localized state. The critical values given by the numerical results are (2D) $\alpha'_c = 6.0$; (3D) $\alpha'_c = 10.28$ and $\alpha'_m = 0.892\alpha'_c$, which are comparable with the results from Gaussian trial wave function method where (2D) $\alpha'_c = 2\pi$; (3D) $\alpha'_c = 10.51$ and $\alpha'_m \approx 0.877\alpha'_c$. Here r and E is in the unit of a_0 and E_0 , respectively.

where $H_{\text{eff}} = -\frac{\hbar^2}{2m_I}\nabla^2 - 2\alpha|\Psi(\mathbf{r}, t)|^2 + 3\beta|\Psi(\mathbf{r}, t)|^4$ and we have a series of soliton solutions (detailed derivation is shown in the supplementary information) $\Psi(\mathbf{r}, t) = \Psi(\mathbf{r} - \mathbf{v}t)e^{i\left[k\cdot\mathbf{r} - \left(\mu + \frac{\hbar^2k^2}{2m_I}\right)t/\hbar\right]}$, where $\mathbf{v} = \hbar\mathbf{k}/m_I$. These soliton solutions are characterized by nonconservative momentum parameter k and excitation energy $E + \frac{\hbar^2k^2}{2m_I}$, identifying that the localized impurity can be represented by a wave packet of length λ moving at a constant speed with the waveform unchanged. In the limit of $\mathbf{v} \rightarrow 0$, the stationary localized impurity wave function $\Psi(\mathbf{r})$ is fully recovered.

Multi-impurity structures. Our theory can be applied to $N(N > 1)$ indistinguishable ultracold impurities and predict some exotic

phenomena. Firstly we consider N noninteracting bosons. Assuming that all the impurities are condensed into a single particle state, i.e., $\Psi_{\text{con}} = \sqrt{N}\Psi_1$, we are able to get the critical value of the localization parameter $\alpha_c(N) = \alpha_c/N$ in 2D, and $\alpha_c(N) = \alpha_c/N^{1/2}$ in 3D (details can be found in the supplementary information), where α_c is the critical value of α in the single-impurity case, independent of N . Therefore, for the noninteracting bosonic impurities, the critical IB interaction for localization is much smaller than single impurity, which is consistent with Ref. 18. For weakly repulsive interacting bosonic impurities, the essential effect of the impurity-impurity interaction $\lambda_{II}\delta(\mathbf{r} - \mathbf{r}')$ is to renormalize the parameter α , and the transition boundary (compared to cases with $\lambda_{II} = 0$) in all dimensions are shifted to $\alpha_c(N) + \lambda_{II}/2$. Specially, a finite value of IB interaction with $\alpha = \lambda_{II}/2$ is now needed to get the impurity localized in 1D.

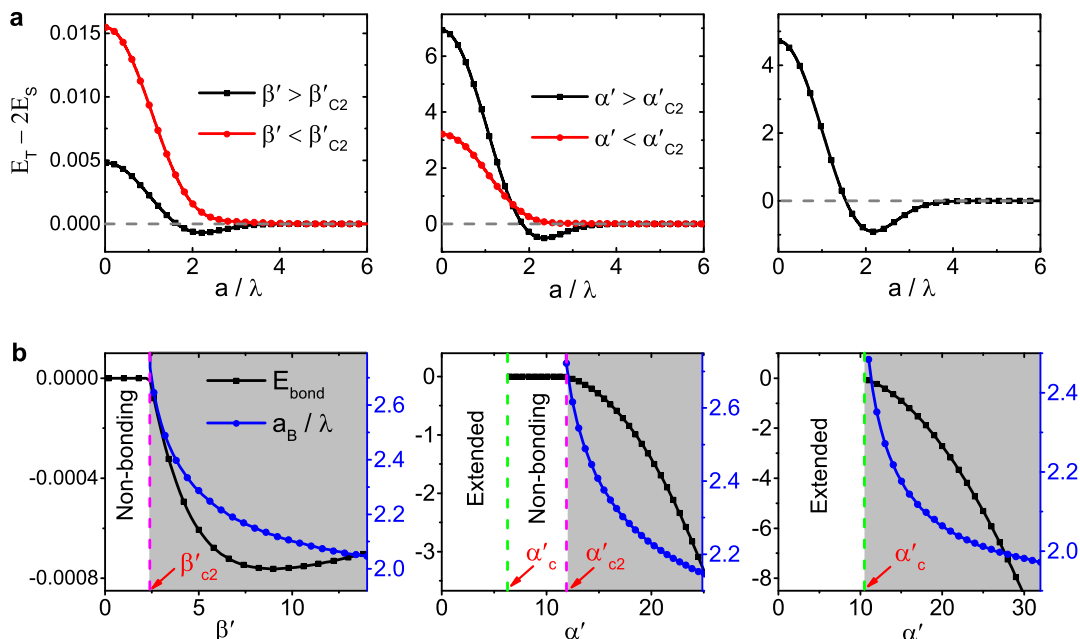


Figure 3 | Two-impurity bonding energy and bonding length. (a), the background mediated impurity-impurity energy $E_T - 2E_S$ for two localized fermionic impurities as function of interimpurity distance in 1D, 2D and 3D (from left to right). (b), the bonding energy E_{bond} and the bonding length a_B as function of dimensionless parameters in 1D, 2D and 3D (from left to right). Notice here E_{bond} is defined as the minimum $E_T - 2E_S$ and a_B is the equilibrium inter-impurity distance. The shadow region marks the parameter space of the formation of the bipolaron. For non-bonding states we have $E_{\text{bond}} = 0$ and the absence of a_B . The numerical results give the critical value $\beta'_{c2} = 2.4$ at 1D and $\alpha'_{c2} = 11.9$ at 2D. a_B/λ decreases when the dimensionless parameters are increased in all dimensions, while E_{bond} shows a non-monotonic behavior in 1D, and at very large β' , E_{bond} approaches zero but still keeps negative, indicating that the bonding state is very weak in this case.

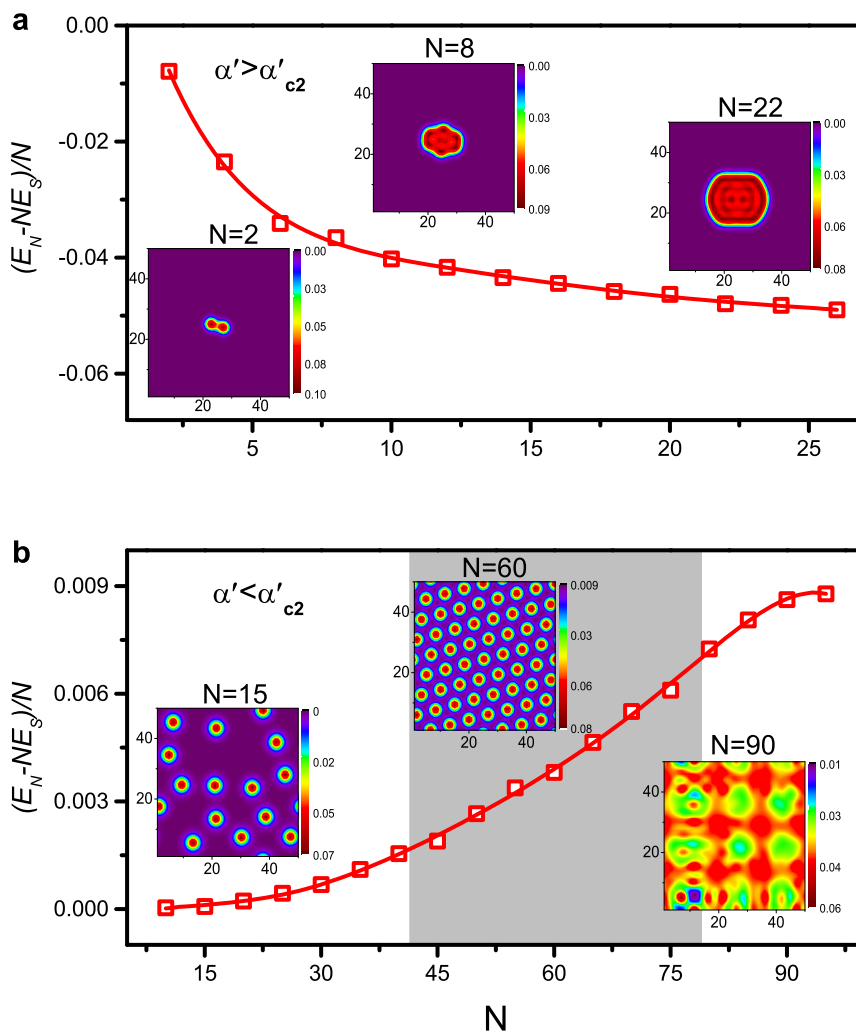


Figure 4 | Multi-impurity structure and indirect impurity-impurity interaction energy. (a–b), plot of indirect impurity-impurity interaction energy per impurity $(E_N - NE_S)/N$ (red solid lines and signals) as function of N in a 2D lattice model with dimensionless parameter (a) $\alpha' = 15.0$, $\beta' = 1.0$, (b) $\alpha' = 7.0$, $\beta' = 1.0$. Here $E_{N,(S)}$ is the total energy for N (single) fermionic impurities, and we use the length and energy unit defined in Table 1. Inset: contour-plot of the impurity density distribution for (a) $N = 2, 8, 22$ and (b) $N = 15, 60, 90$. The shadow region in (b) marks where a stable lattice appears.

Let us now turn our attention to the fermionic impurities. Two localized fermionic impurities are subject to indirect impurity-impurity interactions mediated by the background. This indirect interaction energy can be interpreted as $E_T - 2E_S$, where E_S and E_T are the energies for one impurity and two correlated impurities, respectively. By constructing a bonding and anti-bonding states of two localized wave functions (available in Supplementary Information) with distance between these two localized impurities a as the variational parameter, and considering $E_T - 2E_S$ as function of a , transition between bonding and non-bonding states is found. As we can see from Fig. 3a, there is a critical value of the dimensionless parameter in 1D and 2D, above which two localized impurity can bond together at an equilibrium inter-impurity distance $a = a_B$ with the bonding energy $E_{bond} < 0$. In this case the total energy is lowered when two localized impurities bond together to share the same distortions of the background, and the bound pair can be viewed as an impurity bipolaron. Below the critical value two impurities are non-bonding and shortly repulsive to each other. In 3D bipolaron is always formed as long as the impurities are localized. The two-impurity behaviors in different dimensions, including the boundary between bipolaron and non-bonding state, and behaviors of a_B and E_{bond} are summarized in Fig. 3b.

Different two-impurity behaviors lead to distinct physical configurations for multifermionic impurities. To see this we solve equation (2) self-consistently in a 2D lattice for $N(N > 1)$ fermionic impurities (details available at the Supplementary Information). For a strong IB interaction, while two impurities form a bipolaron, as discussed above, impurities with larger numbers are weakly attractive to each other and form a large impurity molecule (see Fig. 4a). The weak attraction between impurities can also be reflected in the behaviors of the indirect impurity-impurity interaction energy per impurity, which is found to get more attractive (or negative) with N . For a weak IB interaction, the impurities are weakly localized and the impurities are repulsive to each other. As shown in Fig. 4b, for a medium impurity density, the impurities form a triangular lattice structure, while the impurities become randomly distributed for small N and the lattice structure collapses for very large N because the size of the system can not accommodate so many localized impurities. Here the indirect impurity-impurity interaction energy per impurity gets more repulsive as N increases.

As shown in the case with $N = 60$ in Fig. 4b, the total kinetic energy of the impurities is quenched and the short-ranged impurity-impurity interaction becomes dominant and repulsive, which leads to the formation of an impurity lattice. This process is similar to the Wigner



crystallization in solid-state physics. While the Wigner lattice is formed by electrons with long-range Coulomb interactions, the lattice of neutral impurity atoms is due to the IB interaction.

Discussion

We proposed an effective theory for the interaction-induced localization of the ultracold mobile impurities. Beyond its theoretical significance in describing the essential features of the dimension-dependent ELT of the impurity states, our theory also predicted some exotic behaviors of the localized impurities in cold atomic systems, such as molecules and lattice structures, which extends the potential applications of the cold atoms as a quantum simulator for solid-state materials. On the other hand, these features are direct consequences of the impurity effects under the feedback of the background. This is quite different from solid state physics in which the impurity atoms are hardly affected by the background, and marks the unique nature of the mobile impurities. To realize the extended-localized transition and its related phenomena, one may use two-component ^{40}K superfluid as the background and ^6Li as the impurity atom in 2D, since both the ^{40}K superfluid²⁴ and the three-component ^{40}K - ^6Li mixture²⁵ are experimentally accessible. Due to the existence of an energy gap in the spectrum of the background system, the quantum fluctuations and the gapless particle-hole excitations are effectively suppressed, which benefits for the applicability of the meanfield treatment even in low dimensions. As shown in the Supplementary Information, the transition can be achieved by tuning up the scattering length between the impurity and the background to a critical value.

Methods

Derivation of the effective model. To derive model (1), we consider a generic Hamiltonian constructed with three parts:

$$H = \int d\mathbf{r} (h_I + h_B + h_{IB}), \quad (6)$$

where h_I and h_B are local functions of the coordinate \mathbf{r} . h_I is the density of the impurity kinetic energy. h_B contains the kinetic energy density of the background atoms, and the interaction term between the background atoms, which varies for different interacting systems. The IB interaction part is

$$h_{IB} = U_{IB} \hat{n}_I(\mathbf{r}) \hat{n}_B(\mathbf{r}), \quad (7)$$

and it can be rewritten as

$$h_{IB} = U_{IB} \langle \hat{n}_I(\mathbf{r}) \rangle \hat{n}_B(\mathbf{r}) + U_{IB} \langle \hat{n}_B(\mathbf{r}) \rangle \hat{n}_I(\mathbf{r}) - U_{IB} \langle \hat{n}_I(\mathbf{r}) \rangle \langle \hat{n}_B(\mathbf{r}) \rangle \quad (8)$$

in the mean-field level. Within the local density approximation, the local energy density is then given by

$$E(\mathbf{r}) = E_B(\mathbf{r}) \Big|_{\mu_B \rightarrow \mu_B - U_{IB} n_I(\mathbf{r})} + E_I(\mathbf{r}), \quad (9)$$

where $n_{I,B} = \langle \hat{n}_{I,B}(\mathbf{r}) \rangle$, $E_B \Big|_{\mu_B} = \langle h_B \rangle$, $E_I = \langle h_I \rangle$, and μ_B is the chemical potential of the background. By expanding the background energy E_B we get

$$E(\mathbf{r}) = E_I(\mathbf{r}) + E_B(\mathbf{r}) + \sum_m C_m [-U_{IB} n_I(\mathbf{r})]^m, \quad (10)$$

where $C_m = \frac{\partial^m E_B}{m! \partial \mu^m} \Big|_{\mu = \mu_B}$. If the impurity concentration is dilute, i.e., $N/N_B \ll 1$,

where N_B is the total number of the background atoms, the impurities only induce slight changes to the background. In this case it is sufficient to keep $n_I(\mathbf{r})$ to the third order, and get the total energy $E = \int d\mathbf{r} E(\mathbf{r})$ as presented in equation (1) by neglecting impurity-irrelevant terms. The parameters are then given by

$$\alpha = - \frac{\partial^2 E_B}{2 \partial \mu^2} \Big|_{\mu = \mu_B} U_{IB}^2 = \frac{\partial^2 n_B}{2 \partial \mu^2} \Big|_{\mu = \mu_B} U_{IB}^2 \quad (11)$$

$$\beta = - \frac{\partial^3 E_B}{6 \partial \mu^3} \Big|_{\mu = \mu_B} U_{IB}^3 = \frac{\partial^3 n_B}{6 \partial \mu^3} \Big|_{\mu = \mu_B} U_{IB}^3. \quad (12)$$

Clearly for a homogeneous background in the absence of impurities, α , β are \mathbf{r} -independent. For most systems the thermodynamical stability requires a positive α , while the sign of β is largely relevant to the IB interaction and the details of the background.

Length and energy unit. In 1D we define the length unit a_0 and the energy unit E_0 through $\frac{\hbar^2}{2m_1 a_0^2} \sim \frac{\alpha}{a_0}$, and in 2D and 3D they are defined through $\frac{\hbar^2}{2m_1 a_0^2} \sim \frac{\beta}{a_0^2}$ where $l = 2, 3$. Then we get the length and energy unit in Table 1. Accordingly, the parameters α , β have the dimensionless forms α' , β' which are also summarized in Table 1. Notice there is only one independent dimensionless parameter left in each dimension.

	a_0	E_0	α'	β'
1D	$\frac{\hbar^2}{2m_1 \alpha}$	$\frac{2m_1 \alpha^2}{\hbar^2}$	1	$\frac{2m_1 \beta}{\hbar^2}$
2D	$\left(\frac{2m_1 \beta}{\hbar^2} \right)^{\frac{1}{2}}$	$\left(\frac{\hbar^2}{2m_1 \sqrt{\beta}} \right)^2$	$\frac{2m_1 \alpha}{\hbar^2}$	1
3D	$\left(\frac{2m_1 \beta}{\hbar^2} \right)^{\frac{1}{3}}$	$\left(\frac{\hbar^2}{2m_1 \sqrt[3]{\beta}} \right)^{\frac{3}{2}}$	$\alpha \left(\frac{2m_1}{\sqrt[3]{\beta} \hbar^2} \right)^{\frac{3}{2}}$	1

- Schirotzek, A., Wu, C., Sommer, A. & Zwerlein, M. W. Observation of Fermi Polarons in a Tunable Fermi Liquid of Ultracold Atoms. *Phys. Rev. Lett.* **102**, 230402 (2009).
- Zipkes, C., Palzer, S., Sias, C. & Köhl, M. A trapped single ion inside a Bose-Einstein condensate. *Nature* **464**, 388–391 (2010).
- Schmid, S., Härter, A. & Denschlag, J. H. Dynamics of a Cold Trapped Ion in a Bose-Einstein Condensate. *Phys. Rev. Lett.* **105**, 133202 (2010).
- Kohstall, C. *et al.* Metastability and coherence of repulsive polarons in a strongly interacting Fermi mixture. *Nature* **485**, 615–618 (2012).
- Koschorreck, M. *et al.* Attractive and repulsive Fermi polarons in two dimensions. *Nature* **485**, 619–622 (2012).
- Vernier, E., Pekker, D., Zwerlein, M. W. & Demler, E. Bound states of a localized magnetic impurity in a superfluid of paired ultracold fermions. *Phys. Rev. A* **83**, 033619 (2011).
- Jiang, L., Baksmaty, L., Hu, H., Chen, Y. & Pu, H. Single impurity in ultracold Fermi superfluids. *Phys. Rev. A* **83**, 061604(R) (2011).
- Ohashi, Y. Formation of magnetic impurities and pair-breaking effect in a superfluid Fermi gas. *Phys. Rev. A* **83**, 063611 (2011).
- Chevy, F. Universal phase diagram of a strongly interacting Fermi gas with unbalanced spin populations. *Phys. Rev. A* **74**, 063628 (2006).
- Combescot, R., Recati, A., Lobo, C. & Chevy, F. Observation of Fermi Polarons in a Tunable Fermi Liquid of Ultracold Atoms. *Phys. Rev. Lett.* **98**, 180402 (2007).
- Cui, X. & Zhai, H. Stability of a fully magnetized ferromagnetic state in repulsively interacting ultracold Fermi gases. *Phys. Rev. A* **81**, 041602(R) (2010).
- Massignan, P. & Bruun, G. M. Repulsive polarons and itinerant ferromagnetism in strongly polarized Fermi gases. *Eur. Phys. J. D* **65**, 83–89 (2011).
- Mathy, C. J. M., Zvonarev, M. B. & Demler, E. Quantum flutter of supersonic particles in one-dimensional quantum liquids. *Nature Physics* **8**, 881–886 (2012).
- Mahan, G. D. *Many-Particle Physics* (Plenum Press, 2000).
- Cucchietti, F. M. & Timmermans, E. Strong-Coupling Polarons in Dilute Gas Bose-Einstein Condensates. *Phys. Rev. Lett.* **96**, 210401 (2006).
- Kalas, R. M. & Blume, D. Interaction-induced localization of an impurity in a trapped Bose-Einstein condensate. *Phys. Rev. A* **73**, 043608 (2006).
- Sacha, K. & Timmermans, E. Self-localized impurities embedded in a one-dimensional Bose-Einstein condensate and their quantum fluctuations. *Phys. Rev. A* **73**, 063604 (2006).
- Santamore, D. H. & Timmermans, E. Multi-impurity polarons in a dilute Bose-Einstein condensate. *New J. Phys.* **13**, 103029 (2011).
- Bruderer, M., Bao, W. & Jaksch, D. Self-trapping of impurities in Bose-Einstein condensates: Strong attractive and repulsive coupling. *Europhysics Letters* **82**, 30004 (2008).
- Targonska, K. & Sacha, K. Self-localization of a small number of Bose particles in a superfluid Fermi system. *Phys. Rev. A* **82**, 033601 (2010).
- Li, J., An, J. & Ting, C. S. Interaction-induced localization of fermionic mobile impurities in a Larkin-Ovchinnikov superfluid. *Phys. Rev. Lett.* **109**, 196402 (2012).
- Kohn, W. & Sham, L. J. Self-Consistent Equations Including Exchange and Correlation Effects. *Phys. Rev.* **140**, A1133–A1138 (1965).
- Ma, P. N., Pilati, S., Troyer, M. & Dai, X. Density functional theory for atomic Fermi gases. *Nature Physics* **8**, 601–605 (2012).
- Regal, C. A., Greiner, M. & Jin, D. S. Observation of Resonance Condensation of Fermionic Atom Pairs. *Phys. Rev. Lett.* **92**, 040403 (2004).



25. Spiegelhalter, F. M. *et al.* Collisional Stability of ^{40}K Immersed in a Strongly Interacting Fermi Gas of ^6Li . *Phys. Rev. Lett.* **103**, 223203 (2009).

Acknowledgments

This work was supported by the Texas Center for Superconductivity at the University of Houston and by the Robert A. Welch Foundation under Grant No. E-1146. Jin An was also supported by NSFC(China) Project No.1117416.

Author contributions

All the authors contributed equally to this work. All the authors worked closely to propose this study. J.L. and J.A. performed the calculations. J.L., J.A. and C.S.T. analyzed the results and wrote the manuscript.

Additional information

Supplementary information accompanies this paper at <http://www.nature.com/scientificreports>

Competing financial interests: The authors declare no competing financial interests.

How to cite this article: Li, J., An, J. & Ting, C.S. Interaction-induced localization of mobile impurities in ultracold systems. *Sci. Rep.* **3**, 3147; DOI:10.1038/srep03147 (2013).



This work is licensed under a Creative Commons Attribution-NonCommercial-NoDerivs 3.0 Unported license. To view a copy of this license, visit <http://creativecommons.org/licenses/by-nc-nd/3.0>